Determination of the Raman Polarizability Tensor in the Optically Anistropic Crystal Potassium Dihydrogen Phosphate and Its Deuterated Analog

T. Z. Kosc,[1] H. Huang,[1] T. J. Kessler,[1] R. A. Negres,[2] and S. G. Demos[1]

[1]Laboratory for Laser Energetics, University of Rochester
[2]Lawrence Livermore National Laboratory

Potassium dihydrogen phosphate (KDP) and its deuterated analog (DKDP) crystals are widely used nonlinear optical materials in laser applications. They exhibit excellent UV transmission, high damage thresholds and birefringence, and can be grown to large sizes. These properties make them uniquely suited for use in large-aperture inertial confinement fusion (ICF)–class laser systems such as the OMEGA and OMEGA EP lasers and the National Ignition Facility,[1,2] where they are currently used for frequency conversion,[3] polarization control, and beam smoothing.[4] In large-aperture plates, however, the relatively high Raman scattering cross-section of KDP/DKDP supports the generation and transfer of energy to parasitic beams arising from transverse stimulated Raman scattering (TSRS). This effect is of concern in ICF-class lasers due to the high incident laser intensities and long pulse durations that support the exponential increase of the TSRS signal as it traverses the aperture of the crystal plate[5,6] and ultimately leads, if not properly managed, to damage to the optic and the surrounding hardware during laser operation.[7] The TSRS Raman-gain coefficient can be calculated from the propagation length (optic size), the laser intensity and pulse duration, and a complete description of the spontaneous Raman scattering cross section (Raman polarizability tensor).[8,9] The latter is of critical importance to enable one to model TSRS for suitable crystal-cut configurations to help optimize designs. Theory mandates that the Raman tensor is diagonal,[10] but extensive previous efforts yielded results suggesting contributions by off-axis elements.[11,12] This issue has hindered an accurate modeling of TSRS.

In this work, we determine the form of the Raman tensor and identify artifacts that have interfered in previous studies. A unique experimental system developed at LLE employs spherical samples, which enable one to "directly" measure tensor elements through rotation of the sphere to the required scattering geometries.[13] Data were acquired by rotating the sphere through 360° in the azimuthal plane, which is defined as the laboratory x–z plane and contains both the pump-beam propagation and the Raman signal observation directions (Fig. 1). The azimuthal angle $\phi = 0°$ is defined along the laboratory z axis. Laboratory coordinates are defined by lower-case italicized letters x, y, and z, while upper-case letters X, Y, and Z designate crystallographic axes. The experimental notation k_p [e_p e_s] k_s, designates the propagation direction of the pump k_p, and scattered light k_s as well as the unit electric polarization vectors of the pump e_p and scattered light e_s. For clarity, we define the notation for each trace, or set of measurements while the sample is rotated ($\phi = 0°$ to 360°), based on the initial orientation of the sample for $\phi = 0°$ in reference to the crystal axes. Square brackets are omitted in the trace labels in order to differentiate the notation of a data set and specific Raman scattering configurations within that data set.

Three data sets acquired with the crystallographic Z axis, or the optic axis (OA), found in the azimuthal laboratory x–z plane are shown in Fig. 1. The trace labeled ZYYX provides data for scattering in the Z[YY]X configuration at azimuthal angles $\phi = 0°$ and 180°, while scattering data for the X[YY]Z configuration are collected at $\phi = 90°$ or 270°. The polarization orientations of both the pump laser and the Raman scattering signal (and analyzer) for trace ZYYX are perpendicular to the azimuthal plane. A corresponding trace acquired when (a) the analyzer is rotated by 90° (in the azimuthal plane) is shown as ZYZX, and (b) the pump polarization rotated 90° is shown as ZXYX. The signal of the A_1 mode of KDP,[11] centered at 915 cm^{-1}, is integrated between 860 and 960 cm^{-1}. Unexpected features such as double peaks and valleys are detected at the specific angles of importance for determining the matrix elements.

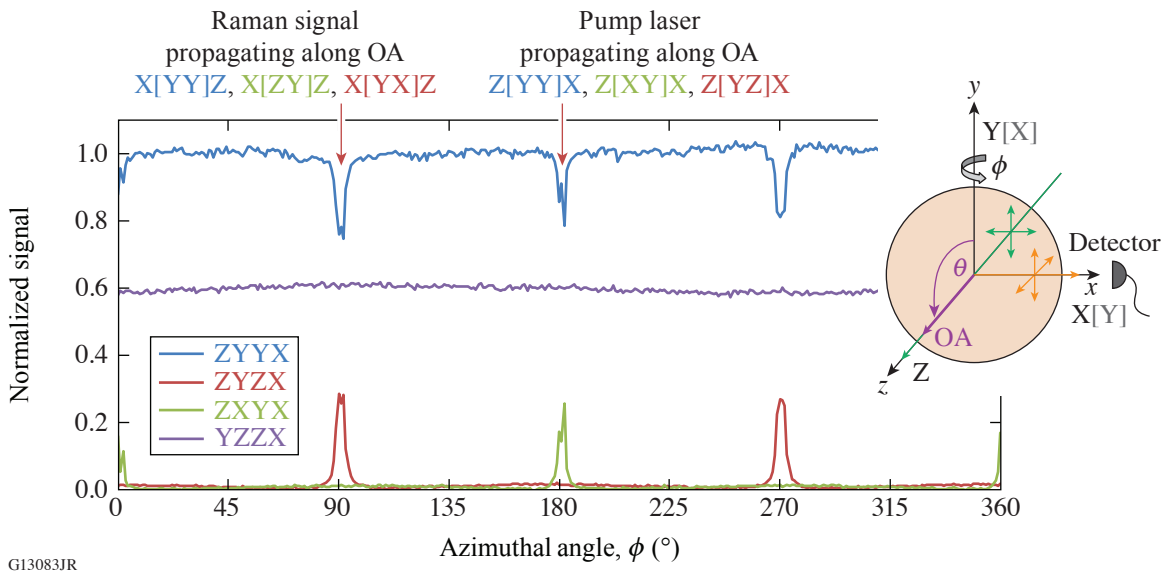

Figure 1
The experimental geometry for Raman scattering measurements is based on a spherical sample (inset). Three traces in which the pump laser and/or the scattering signal propagating along the optic axis experience depolarization are shown. Depolarization artifacts in the form of peaks and valleys arise at azimuthal angles that correspond to configurations at which tensor element values are determined. Data were acquired with an ~1.0° collection half-angle.

These features were reproduced by a ray-trace model that does not consider off-axis tensor elements. The model does consider, however, that in the actual measurement, there is a finite solid angle for the focused laser beam and for the collected Raman scattering. The converging pump laser and the diverging Raman scattering undergo a change of polarization state as a function of propagation length inside the material and orientation of the OA leading to the depolarization of the propagating light. The effect is exacerbated when rays converge or diverge along the OA (because the differential phase between the ray components experiencing the ordinary and extraordinary indices of refraction is the greatest) and increases with the solid angle involved.

Polarization rotation is responsible for the peaks and valleys at critical scattering geometries shown in Fig. 1. The ZYYX trace (blue curve), acquired with the OA lying in the azimuthal plane, should be flat. The polarization, rotation effects observed at $\phi = 0°$ and 180° (Z[YY]X configuration) occur, however, because the vertical polarization of the pump light is altered (i.e., a horizontally polarized component is produced), reducing the amount of Raman signal generated by vertically polarized pump light. An analogous condition exists at $\phi = 90°$ and 270° (X[YY]Z configuration), where the Raman scatter signal propagates along the OA. The Raman scattering signal "lost" to polarization rotation effects appears in configurations for which there should be no Raman scattering from the A_1 mode. Specifically, the slightly wider peaks observed in the ZYZX trace (red) at $\phi = 90°$ and 270° (X[YX]Z configuration) correspond to the polarization rotation of the X[YY]Z configuration exhibiting valleys in the Raman intensity at the same angles. Similarly, the corresponding "lost" signal of the Z[YY]X configuration appears as sharp narrow peaks in the ZXYX trace (green) at the same azimuthal angles (Z[XY]X configuration). Here the polarization rotation of the pump light generates a Z[YY]X component that gives rise to the observed signal where no signal should be found. Note, that data were collected at the smallest-possible collection angle to minimize polarization rotation artifacts.

A closer examination of the Raman scattering spectral profile in the 860- to 960-cm^{-1} integration region for all spectra within each data set led to the identification of additional Raman modes whose spectral profiles partially overlap into the wave number range considered for the determination of the intensity of the 915-cm^{-1} mode. Spectra for the YZZX trace, which includes both Y[ZZ]X and X[ZZ]Y configurations, all show the same strong 915-cm^{-1} peak (Fig. 2). Configurations corresponding to the ZYXY trace, Z[YX]Y and Y[ZX]Z, determine off-axis tensor elements and should not generate a scattering signal. Spectral analysis confirmed that the strong peaks at $\phi = 0°$ and 180° in the ZYYX trace are due to a 915-cm^{-1} peak arising from depolarization effects. The spectrum for the X[ZY]Z configuration reveals that Raman scattering from additional low-intensity modes adjacent

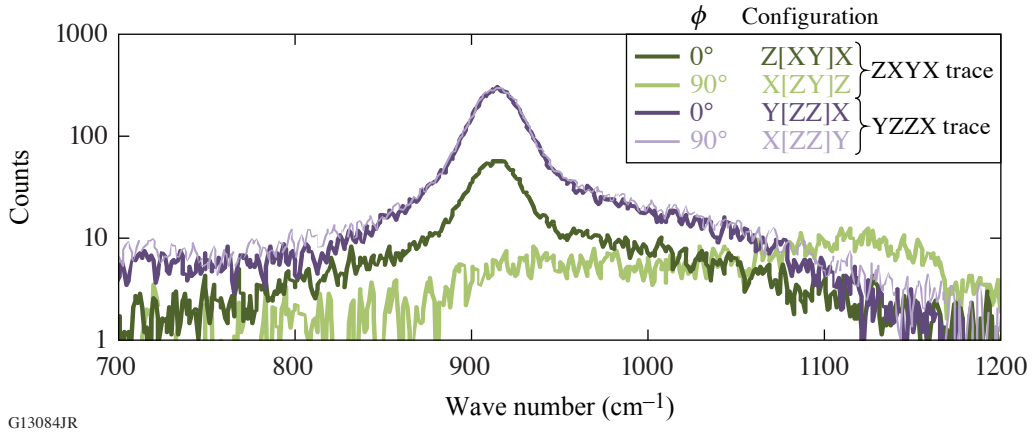

Figure 2
Selected spectra at 0° and 90° demonstrate the presence of Raman scattering from the dominant A_1 mode of KDP (trace YZZX) and the depolarization and the overlap of neighboring modes (trace ZXYX). Data acquired with an ~0.5° focusing half-angle and 1.0° collection half-angle.

to the 915-cm^{-1} mode overlap with the integration region and give rise to erroneous signals that can be misinterpreted as arising from nondiagonal matrix elements.

The theoretical description of the Raman tensor R for the A_1 mode is represented by a diagonal matrix.[13] In the following analysis, all other tensor elements are normalized to the value of A, which is assigned the maximum value of trace ZYYX (or ZXXY). The matrix element B is determined solely by averaging of the entire trace YZZX. The examination of spectra for all experimental configurations confirmed that the Raman tensor for the dominant A_1 mode contains no off-axis terms. The same analysis was performed for both KDP and 70% DKDP samples tested in an experimental setup using a 1.0° collection half-angle. Future work will explore the dependence of the collection aperture on the tensor element values more carefully.

$$R(\mathrm{A_1}) = \begin{pmatrix} A & 0 & 0 \\ 0 & A & 0 \\ 0 & 0 & B \end{pmatrix} \quad R_{\mathrm{KDP}} = \begin{pmatrix} 1 & 0 & 0 \\ 0 & 1 & 0 \\ 0 & 0 & 0.79 \pm 0.01 \end{pmatrix} \quad R_{70\%\ \mathrm{DKDP}} = \begin{pmatrix} 1 & 0 & 0 \\ 0 & 1 & 0 \\ 0 & 0 & 0.76 \pm 0.02 \end{pmatrix}.$$

This material is based upon work supported by the Department of Energy National Nuclear Security Administration under Award Number DE-NA0003856, the University of Rochester, and the New York State Energy Research and Development Authority.

1. J. D. Lindl *et al.*, Phys. Plasmas **11**, 339 (2004).
2. N. Fleurot, C. Cavailler, and J. L. Bourgade, Fusion Eng. Des. **74**, 147 (2005).
3. W. Seka *et al.*, Opt. Commun. **34**, 469 (1980).
4. T. R. Boehly *et al.*, J. Appl. Phys. **85**, 3444 (1999).
5. C. E. Barker *et al.*, Proc. SPIE **2633**, 501 (1995).
6. S. N. Dixit *et al.*, J. Phys. IV France **133**, 717 (2005).
7. K. R. Manes *et al.*, Fusion Sci. Technol. **69**, 146 (2016).

8. Y. R. Shen and N. Bloembergen, Phys. Rev. **137**, A1787 (1965).

9. A. Z. Grasiuk and I. G. Zubarev, Appl. Phys. **17**, 211 (1978).

10. R. Loudon, Adv. Phys. **13**, 423 (1964).

11. W. L. Smith, M. A. Henesian, and F. P. Milanovich, *Laser Program Annual Report 1983*, 6-61, Lawrence Livermore National Laboratory, Livermore, CA, Report UCRL-50021-83 (1984).

12. S. G. Demos *et al.*, Opt. Express **19**, 21050 (2011).

13. T. Z. Kosc *et al.*, Rev. Sci. Instrum. **91**, 015101 (2020).

Long-Term Monitoring of the Damage Performance of Multilayer Dielectric Grating Samples Residing Inside the Compressor Chamber of the OMEGA EP Laser

A. A. Kozlov, S. G. Demos, D. Canning, B. N. Hoffman, B. E. Kruschwitz, A. L. Rigatti, and L. J. Waxer

Laboratory for Laser Energetics, University of Rochester

The laser-induced–damage threshold (LIDT) of the final transport optics is a critical factor limiting the output energy in ultrahigh-power lasers (e.g., OMEGA EP) based on chirped-pulse amplification. The multilayer dielectric (MLD) gratings in such laser systems are expensive, hard to manufacture/replace, and highly susceptible to laser-induced damage.[1] Two pulse compressors on OMEGA EP are stacked vertically in a single grating compression chamber (GCC) having internal dimensions of 4.57 m × 4.57 m × 21.34 m (15 ft × 15 ft × 70 ft) and operating under nominal vacuum of 2×10^{-6} Torr. The GCC is populated with over 100 optomechanical structures, control devices, and optical components and vented for quarterly maintenance. Although all materials and manufacturing processes used in the OMEGA EP vacuum systems are subject to approval through a qualification process,[2] it is necessary to monitor in-vacuum LIDT for optical components residing inside the GCC to ensure the failure-free and cost-effective operation of the laser. Since the OMEGA EP Laser System is designed to operate in a wide range of pulse durations (from about 500 fs up to 100 ps), the recent discovery that more than one type of defect species can initiate damage in regimes[3] of different pulse lengths has made the continuous evaluation of the LIDT more complex than originally anticipated.

A special protocol for a long-term damage testing campaign was established on OMEGA EP from the beginning of GCC population to monitor the damage performance of representative optics under exposure to the vacuum chamber environment. A set of small-size optics samples was selected and placed inside the GCC during normal operation, and routinely tested for damage on every quarterly GCC vent using the in-house short-pulse damage testing system. The samples were positioned near the most-critical optical elements and in areas undergoing the most intense maintenance activities. Over the last ten years, the long-term campaign was divided into three smaller campaigns.

The Round I Campaign (2007–2010) started using a set of development MLD gratings. Damage testing at a 600-fs pulse length showed no changes in the damage performance. The damage testing results at a 10-ps pulse length showed no significant change for 15 of the grating samples used during the GCC population period. A decline was observed, however, for three gratings. Due to the extensive damage testing schedule, only one grating sample remained under monitoring for the remainder of the Round I Campaign. This grating showed a 30% decline in the 10-ps damage testing results after three years of vacuum exposure inside the GCC.

The Round II Campaign (2010–2016) utilized three production witness grating samples (denoted as II-1, II-2, and II-3) and involved damage testing at a 10-ps pulse length in vacuum. The damage testing results for this round are summarized in Fig. 1(a). Variations in the LIDT values, observed over this six-year test period, may be separated into two regimes: (1) during the first three years where changes were small and (2) during the following three years where a considerable decline was observed. These results must be evaluated, taking into account that the system was in full operational mode during the period of the most LIDT decline. Overall, the 1-on-1 and *N*-on-1 thresholds dropped by ~40% concurrently. In addition, the online grating inspection system[4] on OMEGA EP detected damage onset during operation at a 100-ps pulse length at a fluence level significantly below the initial damage threshold measured using the production witness grating samples. Near the end of Round II testing, the LIDT's of all grating samples at 100 ps were similar to those at a 10-ps pulse length.

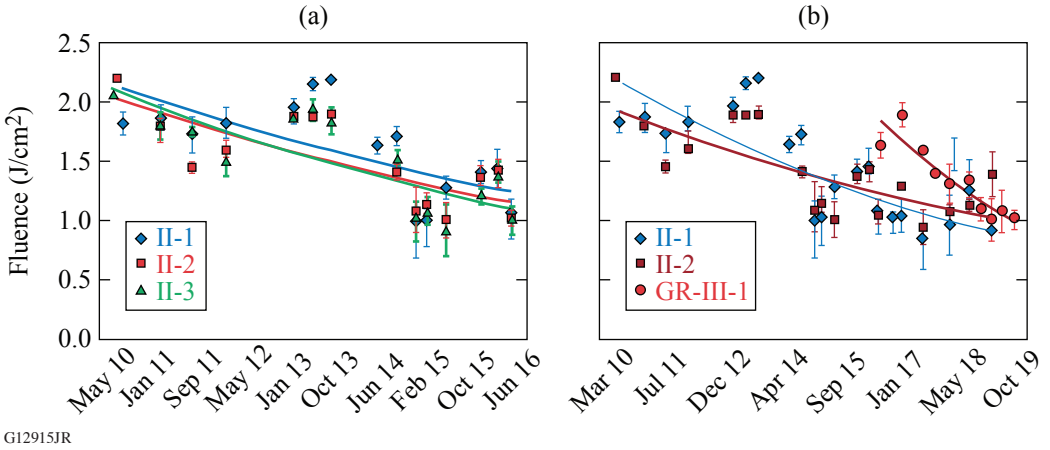

Figure 1
(a) The Round II and (b) Round III, *N*-on-1 damage testing results.

The Round III Campaign (2016–2019) encompassed an expanded protocol to monitor damage testing at a 100-ps pulse length. A "fresh" grating sample (GR-III-1) and the representative grating high-reflector (GHR) coating (HR-III-1) were included in the experiment to study potential differences in the vacuum performance between the MLD gratings and regular coatings. The representative grating high reflector is identical to the regular grating MLD coating with the exception of the top silica layer, which has a reduced thickness (609 nm to 440 nm) and no etched grating structure. To separate the vacuum effects from the aging-related changes in the optics performance, the fresh grating and coating samples had an equivalent twin (GR-III-2 and HR-III-2, respectively) that was stored in air throughout the campaign. Furthermore, one sample (II-3) from the Round II Campaign was removed from the study and stored in air.

Figure 1(b) summarizes the 10-ps-pulse-length damage testing results obtained during the Round III campaign combined (to enable direct comparison) with the data from Round II. Both 1-on-1 and *N*-on-1 damage thresholds for the fresh grating sample GR-III-1 were reduced by 40% over three years. This decline is exactly the same as the reduction of the damage threshold experienced by the gratings II-1 and II-2 during Round II, but it occurred twice as fast. The 10-ps damage thresholds for these two remaining Round II grating samples continued to decline during Round III with the 1-on-1 and *N*-on-1 LIDT reduced by 20% and 10%, respectively. However, the damage thresholds for the Round II gratings II-1 and II-2 showed no further measurable decline at the 100-ps pulse length.

Damage testing results at a 100-ps pulse length of Round III, GCC-stored fresh grating GR-III-1 are presented in Fig. 2, combined for comparison with the 10-ps data for the same sample. The damage testing results at a 100-ps pulse length for the fresh grating GR-III-1 declined significantly faster in comparison with the 10-ps data. Specifically, the 100-ps 1-on-1 and *N*-on-1 damage thresholds dropped by ~50% and ~70%, respectively. As a result, the damage threshold at 10 ps and 100 ps converged. On the other hand, no convergence between 10-ps and 100-ps damage thresholds was observed for grating GR-III-2, which was stored in air.

The GHR coating sample HR-III-1, stored inside the GCC, showed no change in damage thresholds at 10 ps, but the damage behavior changed significantly at a 100-ps pulse length. The 1-on-1 damage threshold at 100 ps dropped by ~50% after three years in vacuum, while the *N*-on-1 remained unchanged.

The overall percentage decline in the damage thresholds in all, GCC and in-air stored, samples (Fig. 3) depicts a clear difference in the vacuum damage performance between the MLD gratings and GHR coatings. The damage thresholds of the MLD's grating were reduced in vacuum by up to 70%, depending on the pulse length. For the GHR coatings, only the 1-on-1 damage threshold at a 100-ps pulse length was affected by the environment inside the GCC. Both grating and GHR-coating samples revealed no change in the damage performance after three years of aging in ambient air.

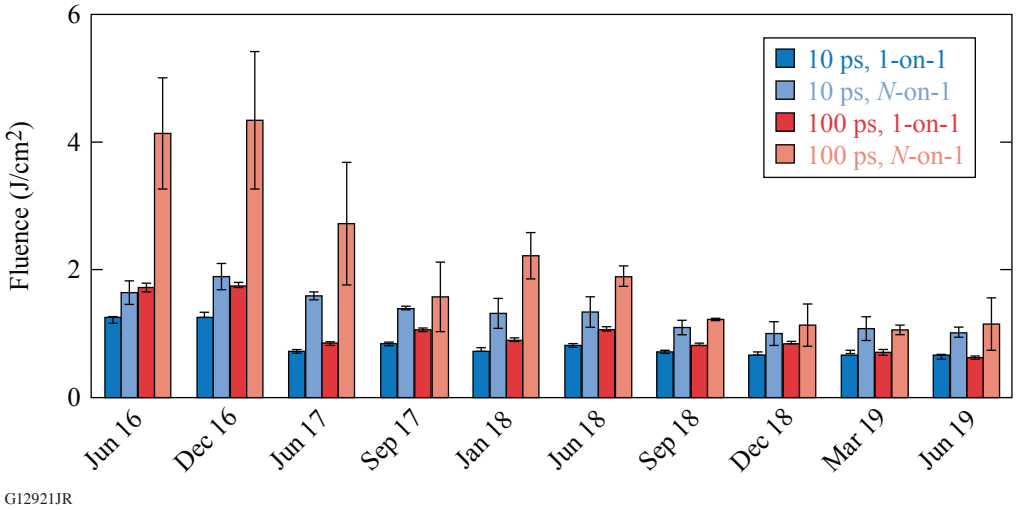

Figure 2
Round III, "fresh" grating GR-III-1: The 10-ps and 100-ps damage thresholds converged under vacuum exposure inside the GCC.

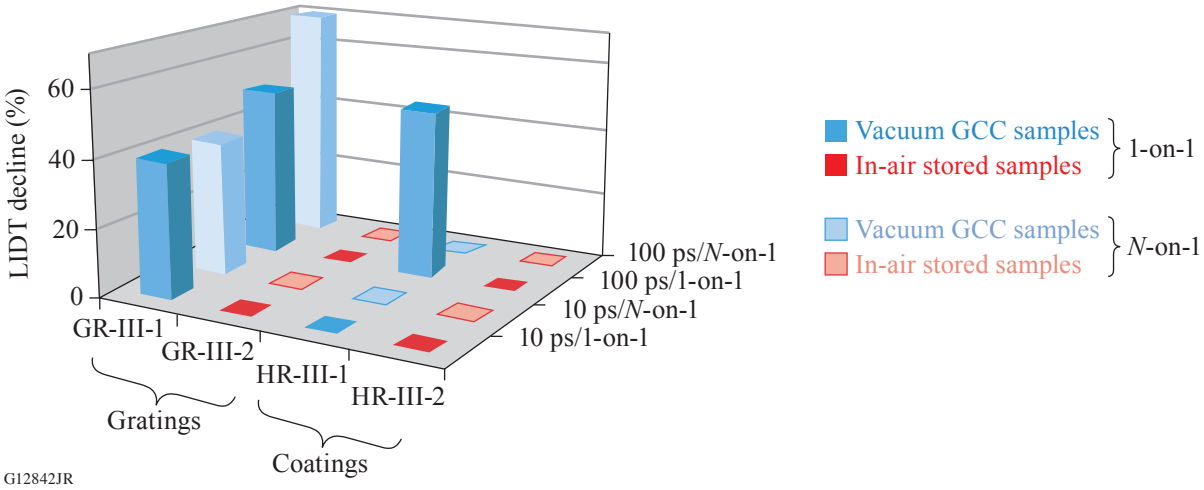

Figure 3
The evolution of the damage performance of the MLD-grating and GHR-coating samples during Round III.

Surface plasma cleaning was used on grating sample II-3 to target potential organic volatile contaminants, presumably accumulated on the grating surface under vacuum inside the GCC.[5] The results indicated that the air–plasma cleaning method did not improve the damage performance of the grating. This suggests that the degradation of the grating damage performance under vacuum conditions inside the GCC is not related to volatile organic contamination.

Particles that attach to the surface of optics (contaminants) can be precursors for damage initiation on these optics at significantly lower fluences than the corresponding pristine optical elements. Offline studies have shown that particles on the surface can significantly lower the damage thresholds.[6] It is currently unclear, however, what types of particles may be present inside

the GCC and if they correlate with the reduced damage performance of the compression gratings discussed in this work. In an effort to perform a preliminary analysis of the contamination load inside the OMEGA EP GCC, particles were collected from seven locations near optical elements during the December 2019 vent period. The initial analysis was focused on determining the particle composition and was limited to the larger particles (>50 μm diameter). Particles were found at every collection location with the most frequently observed type being metallic particles and fibers, for the subset of particles that were chemically characterized. Several different metal particles were identified, including aluminum, stainless steel, silver, and copper. Plastic (PVC) particles were also found near the compressor grating and the lower compressor deformable mirror. Glass particles were less commonly observed.

Differences in damage degradation behavior between the MLD grating and corresponding GHR coating may arise from the different damage initiation mechanisms. As reported in Ref. 3, the damage of HfO_2/SiO_2–based HR's by laser pulses longer than 10 ps is defect-driven Type II or Type III, originating at depths around 600 nm and >100 nm, respectively. Conversely, damage initiation in gratings with picosecond pulses originates in the pillars (the location of peak electric-field intensity enhancement) and is associated with defect-induced localized absorption.[7] Therefore, damage in the MLD grating and the GHR coating occurs at different locations. The damage-initiation mechanisms described above apply for the case of the "pristine" optic (grating or GHR coating). Assuming there is contamination involved, the problem becomes more complex and would require additional studies to resolve. However, the existing results may help obtain insight into the possible processes.

Recent work that considered the interaction of model contamination particles (metal, plastic, and glass) located on the surface on an MLD mirror with pulses at 0.6 and 10 ps revealed that the threshold for metal particle ejection and secondary contamination (via nanodroplets) is largely dependent on only the fluence.[6] These processes take place at fluences below the particle-induced LIDT of the mirror. If we further consider that damage is initiated by the generated (secondary contamination) nanoparticles, due to their small size, heat diffusion would be limited and damage would be only a function of total fluence. This would explain the convergence of the 100-ps 1-on-1 LIDT toward the 10-ps 1-on-1 LIDT (as depicted in Fig. 2). Regarding the behavior of the grating samples, the introduction of metal contamination particles would alter the localized electric-field distribution near the pillars creating "hot" spots with higher electric-field intensity. This in turn would facilitate a reduction of the LIDT. Additional work would be required to validate the above hypothetical.

This material is based upon work supported by the Department of Energy National Nuclear Security Administration under Award Number DE-NA0003856, the University of Rochester, and the New York State Energy Research and Development Authority.

1. N. Bonod and J. Neauport, Adv. Opt. Photon. **8**, 156 (2016).

2. B. Ashe *et al.*, Proc. SPIE **7069**, 706902 (2008).

3. A. A. Kozlov *et al.*, Sci. Rep. **9**, 607 (2019).

4. J. Qiao *et al.*, Opt. Express **18**, 10,423 (2010).

5. H. P. Howard *et al.*, Appl. Opt. **52**, 1682 (2013).

6. K. R. P. Kafka and S. G. Demos, Opt. Lett. **44**, 1844 (2019).

7. B. N. Hoffman *et al.*, "Mechanisms of Picosecond Laser-Induced Damage in Common Multilayer Dielectric Gratings," to be published in Optics Express, see also, this issue of LLE Review Quarterly Report **162**, 77.